InGaN islands and thin films grown on epitaxial graphene

C Paillet, S. Vézian, C. Matei, A. Michon, B. Damilano, A. Dussaigne, B Hyot

InGaN islands and thin films grown on epitaxial graphene

C. Paillet,[1,2] S. Vézian,[2] C. Matei,[1] A. Michon,[2] B. Damilano,[2] A. Dussaigne,[1] B. Hyot[1]

[1]*Université Grenoble Alpes, CEA-LETI, 17 Avenue des Martyrs, F-38054 Grenoble, France*

[2]*Université Côte d'Azur, CNRS-CRHEA, rue Bernard Gregory, 06560 Valbonne, France*

Abstract

In this work is studied the growth of InGaN on epitaxial graphene by molecular beam epitaxy. The nucleation of the alloy follows a three-dimensional (3D) growth mode, in the explored temperature range of 515-765°C, leading to the formation of dendrite-like islands. Careful Raman scattering experiments show that the graphene underneath is not degraded by the InGaN growth. Moreover, lateral displacement of the nuclei during an atomic force microscopy (AFM) scan demonstrates weak bonding interactions between InGaN and graphene. Finally, a longer growth time of the alloy gives rise to a compact thin film in partial epitaxial relationship with the SiC underneath the graphene.

1. Introduction

The growth of III-N semiconductors is very often made on hetero substrates, as no bulk III-N subtrates are affordably available. Therefore, the growth of III-N materials is usually performed on sapphire or SiC [1]. However, these substrates induce strain in the grown material, which can become highly detrimental when it comes to build a device. For instance, Lymperakis et al. [2] demonstrated that under a strained growth regime, InGaN alloy will inevitably undergo chemical re-ordering, and will therefore have compositional inhomogeneities, when its In concentration is above 25%at. Nonetheless, thanks to the recent developments in 2D materials synthesis [3–5], one could think of suppressing the strain in the deposited materials by using dangling bonds free substrates. Indeed, it is

not expected that chemical bonds would form between the substrate and the grown material. Moreover, it has already been shown that the 3D deposited material can grow in epitaxial relationship with the bulk substrate supporting the 2D layer [6,7] during a process named 'van der Waals epitaxy' or 'remote epitaxy'. Additionally, the interest of such epitaxial process would be the ease in lifting off the deposited material or even a complete device structure from the substrate leaving the 2D layer available for another growth over several cycles [7–9]. In this manner, the growth of III-N materials on graphene has been studied during the last decade, with a focus on GaN, demonstrating the possibility to grow thin films [6,8,10–13]. However, in these studies, it is not always clear whether the graphene is damaged or not, and consequently if the nucleation occurs on the graphene or through it onto the supporting substrate. Other studies present the elaboration of micro or nanostructures like columns [14–17] and islands [18–20]. With such morphologies, the study of the graphene layer quality after the growth is more straightforward and it was revealed that the graphene is often damaged [15–19]. Indeed, the nucleation has been shown to generally occur around defected area of the graphene due to the exposition to a plasma [15,19] or due to the high growth temperatures combined with harsh gas environment [21]. Nonetheless, Journot et al. [18] could unambiguously differentiate morphologies of GaN islands, nucleating either on the graphene or on the substrate through a hole in the graphene, depending on their growth process. They could also evidence weak bonding interactions for islands grown on graphene and control their orientation.

Herein, is presented the nucleation and growth of InGaN by molecular beam epitaxy (MBE) on epitaxial graphene. First, the nucleation of InGaN is investigated as a function of the growth temperature. The growth of InGaN islands is demonstrated while preserving the graphene layer quality as shown by Raman spectroscopy. Moreover, weak bonding interactions are evidenced between the islands and the graphene substrate. Finally, the growth of the III-N semiconductor is extended to synthesize a film whose structural and optical properties are studied.

2. Methods

The epitaxial growth of graphene is conducted by propane based chemical vapour deposition (CVD) on the Si-face of 1 x 1 cm^2 6H-SiC substrates provided by TankeBlue with a 0.1° miscut angle along the $< 11\bar{2}0 >$ direction. The SiC substrates are placed in a resistively heated tubular chamber where they are first annealed for 5 minutes at 1450°C and 800 mbar under an Ar/H_2 atmosphere. This annealing leads to the formation of steps in the SiC substrate [22] toward the orientation of the miscut angle. Following this, the propane flow in the chamber is set to 10 sccm for 5 minutes under the same conditions. It results in the formation of an atomically flat graphene layer over the entire substrate's stepped surface as shown in **Figure 1(a)** with topographic atomic force microscopy (AFM) image in tapping mode using a Digital Instruments Dimension 3100 AFM microscope from Veeco mounted with a Si tip. The white arrows indicate the crystallographic orientation of the SiC substrate. After the complete coverage of the surface by the graphene, no additional growth occurs on the sample meaning that it is a self-limiting process. The graphene layer is actually laying on a carbon layer partially bonded to the substrate, called buffer layer [23,24], as depicted in **Figure 1(b)**. The low-energy electron diffraction (LEED) pattern of the sample, in **Figure 1(c)** indicates a 30° rotation of the monoatomic carbon layer (orange arrows) relatively to the SiC substrate (green arrows). To estimate the quality of the graphene layer, Raman spectroscopy was performed using a Raman InVia microscope from Renishaw equipped with a 1800 $gr.cm^{-1}$ diffraction grating and working with a 532 nm laser focused on the surface thanks to a x100 optical microscope objective. In our case, the Raman spectrum of the epitaxial graphene in **Figure 1(d)** displays the well-established 2D (ω_{2D} = 2686 cm^{-1}) and G (ω_G = 1588 cm^{-1}) peaks [25] after subtraction of the SiC background. Both G and 2D peaks are very sharp with respectively 9 cm^{-1} and 24 cm^{-1} full width at half maximum (FWHM). Moreover, no D peak (expected around 1350 cm^{-1}) related to the defects is observed on the spectrum. Altogether, these features demonstrate a good structural quality of the graphene layer. The small bump arising at around 1500 cm^{-1} can be attributed to the presence of the buffer layer underlying the graphene [26–29].

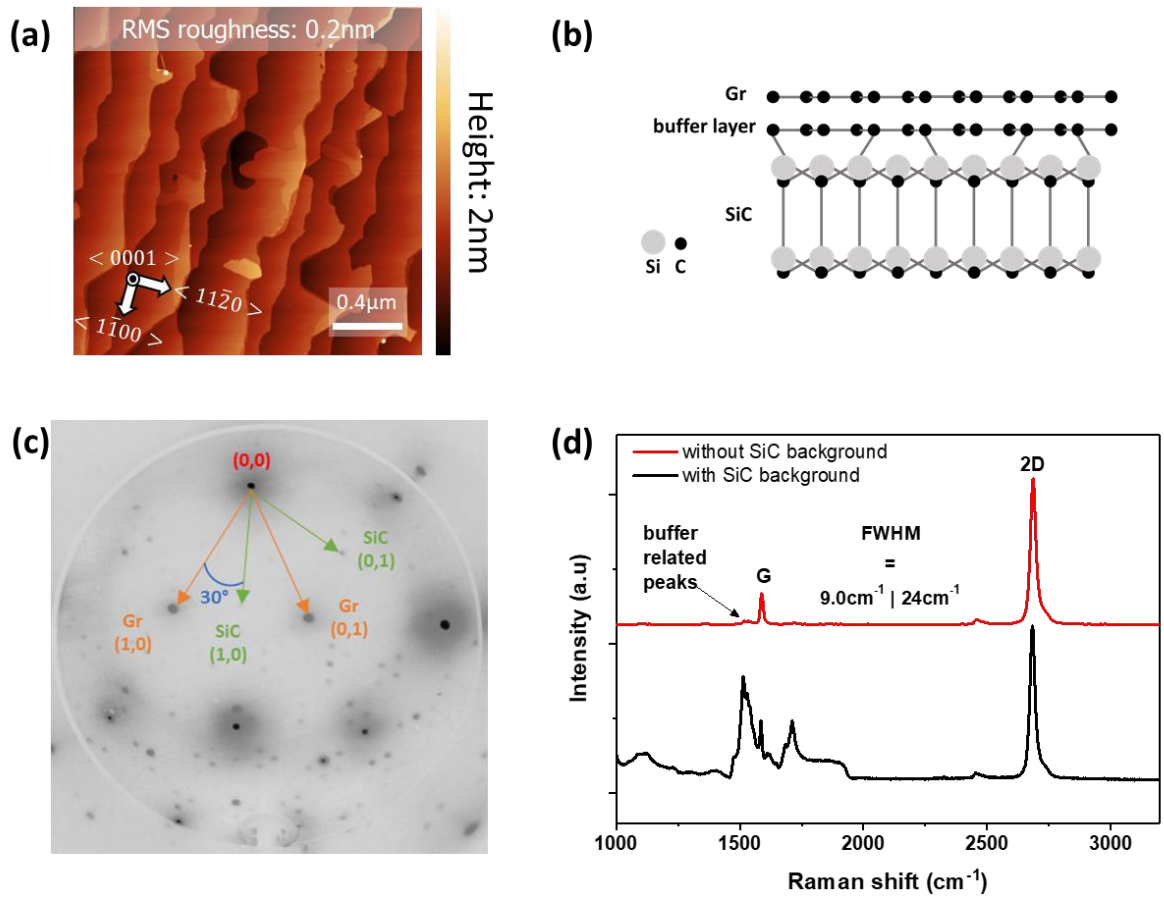

Figure 1: *(a) Topographic atomic force microscopy (AFM) image in tapping mode of epitaxial graphene on 6H-SiC, with white arrows indicating the crystallographic orientation of the SiC substrate. (b) Schematic structure of the buffered graphene layer on 6H-SiC. (c) Low energy electron diffraction pattern (LEED) of graphene/SiC obtained at 140 eV (image processed to enhance the contrast), with orange and green arrows indicating respectively reticular planes from the graphene and the SiC relatively to the origin point (marked in red). (d) Raman spectrum of epitaxial graphene on SiC probed with a 532 nm laser before (black) and after (red) subtraction of the SiC background.*

The growth of InGaN on the aforementioned epitaxial graphene is operated in ultra-high vacuum (UHV) in a Riber 32P MBE system equipped with In and Ga effusion cells and a NH_3 gas line. The respective beam equivalent pressures used for In and Ga were 7.0 x 10^{-8} Torr and 2.4 x 10^{-7} Torr. The ammonia flux was 500 sccm. The chamber also comprises a reflection high-energy electron diffraction (RHEED) apparatus working at 15 kV and 1.6 A to follow in situ the growth process. The 1x1 cm^2 sample is mounted within the reactor on an In-free substrate holder heated by a oven.

Samples were characterized by scanning electron microscopy (SEM) with a Zeiss Supra 40 at 5 kV using an Everhart-Thornley secondary electron detector. X-ray diffraction measurements were conducted

with a Panalytical X'Pert Pro MRD diffractometer using the Cu Kα emission line at 1.5406 Å. Photoluminescence experiments were achieved using a frequency-doubled Ar laser at 244 nm, a 150 $gr.mm^{-1}$ grating and a Si CCD. Finally, electron backscatter diffraction (EBSD) was done in a Zeiss Merlin microscope equipped with a Bruker QUANTAX e^{-}Flash EBSD detector at 20 kV and a 70° angle incidence of the electron beam related to the sample. The analysis of the data was performed using the dedicated Esprit software from Bruker.

3. Results and discussion

3.1 InGaN nucleation

The growth of a 3D material on a 2D substrate is unambiguously different than on a conventional 3D substrate and therefore needs an extended study of the growth conditions to perform the nucleation and later on the growth of a thin film. The lack of dangling bonds on the surface leading to a very low reactivity reduces the probability for an incoming atom to adsorb on the surface and lower the gas molecules cracking rate. The nucleation of InGaN by MBE has been investigated at 515°C, 685°C and 765°C for a constant duration of 15 minutes. **Figure 2** depicts the three different morphologies observed by SEM for each temperature studied. The growth at the lowest temperature (i.e. 515°C), induces the formation of metallic droplets indicated by white round particles in **Figure 2(a)**, due to metal accumulation. Indeed, as the temperature is decreased, the cracking efficiency of ammonia becomes too low to provide enough reactive nitrogen to adsorb on the graphene and react with In and Ga to initiate the growth. The excessive metallic atoms are therefore agglomerating into droplets. Increasing the temperature can be a way to tackle this problem by enhancing the decomposition of ammonia. Nonetheless, raising it too much can also have detrimental effect on the growth. For instance, when performed at 765°C, the nucleation of InGaN appears to be very slow, as shown in **Figure 2(c)** where the grown nuclei are rather small (less than 1 µm). Here, the adsorption of In, Ga

and N on the graphene surface is very low and limits the growth rate. The growth must be then conducted at an intermediate temperature (685°C) to obtain a convenient growth rate while avoiding droplets formation. The nucleation of InGaN on graphene takes place through a 3D growth mode by randomly forming dendrite-like islands as displayed in **Figure 2(b)**. These islands are made of interlocked triangles and measure roughly 1 to 4 µm along their longest direction and 20 to 40 nm in height (determined by AFM). It is not yet explained why the InGaN nuclei adopt these shapes at the first stages of the growth. However, a derived diffusion-limited aggregation (DLA) model developed by Bartelt and Evans [30] to study metal-on-metal epitaxy of Pt/Pt(111) evidenced similar island morphologies varying from narrow dendrite branches to more or less compact interlocked triangles depending on the adatoms mobility. In this model, the incoming adatoms randomly travel on the surface until they encounter an already formed nucleus. While being incorporated in the island, the adatoms are still able to jump from one site to another along its edges until they permanently bond at a kink or to another moving adatom.

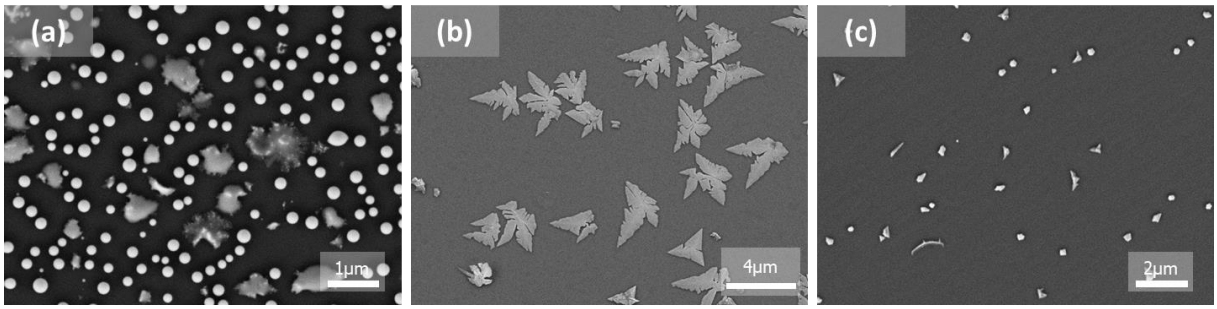

Figure 2: *Secondary electron microscopy (SEM) images of InGaN nucleation on epitaxial graphene on 6H-SiC by molecular beam epitaxy (MBE) at (a) 515°C, (b) 685°C and (c) 765°C for 15 minutes.*

3.2 Properties of graphene after the growth

After observing the nucleation of InGaN on graphene, it is essential to characterize the 2D graphitic material again to assess the impact of the InGaN growth on its structural quality. The graphene is therefore probed by Raman spectroscopy mappings in a 14.5 x 14.5 µm² area with 0.5 µm steps (i.e. totalizing 900 spectra) for the sample processed at 685°C. After the growth, **Figure 3(a)** and **Figure 3(b)** display respectively the probed area observed by SEM denoted by a red dashed box and the associated

mapping of the position of the graphene G peak. The position of the G peak (ω_G) in **Figure 3(b)** follows the shape and the position of the InGaN islands on the graphene while it is clearly not the case for the position of the 2D peak (ω_{2D}) in **Figure 3(c)**. G peak seems to undergo a systematic blue shift in areas covered by InGaN.

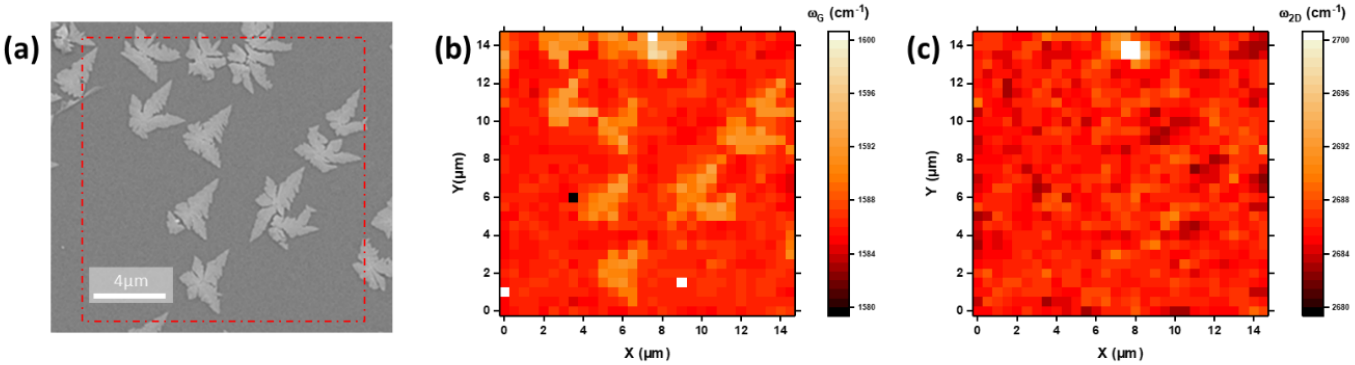

Figure 3: *(a) Secondary electron microscopy (SEM) image of InGaN nucleated at 685°C with a red dashed box indicating the area probed for the associated Raman spectroscopy mapping of (b) G peak position (ω_G) and (c) 2D peak position (ω_{2D}) of graphene underneath.*

It has already been reported in literature that both strain [31] and doping [32–34] of graphene lattice influence the position and width of G and 2D peaks. Thus, it is not always clear whether the shift of the graphene characteristic peaks comes from strain, doping or even both at the same time. However, Lee et al. [35] were able to decouple the influence of strain and doping on the shift of these peaks. They plotted ω_{2D} against ω_G for several spectra obtained for different graphene samples with various strain and doping states. These points were plotted relatively to the position of the G and 2D peaks of a pristine graphene sheet free of strain and doping. They showed that starting from this reference point, a new coordinate system could be built with axes representing strain and doping contribution on ω_{2D} and ω_G. In our case, ω_{2D} and ω_G values of each spectrum were extracted and then plotted in **Figure 4(a)**. Two point clouds can be identified, a first one (200 orange points), corresponding to graphene area covered by InGaN, and a second one (700 red points) corresponding to uncovered graphene. The reference point (pink rotated square) is taken from Das et al. [36] with ω_G^0 = 1683 cm^{-1} and ω_{2D}^0 = 2678 cm^{-1}. The axis related to the strain (black line) follows a linear slope $\Delta\omega_{2D}/\Delta\omega_G \approx 2.2$ [35,37]. A blue shift

of the peaks corresponds to a compressive state of the graphene layer and a red shift is due to a tensile state. The p-doping contribution axis (blue line) follows the slope $\Delta\omega_{2D}/\Delta\omega_G \approx 0.55$ [37,38] and the n-doping contribution (dark green line) follows the slope $\Delta\omega_{2D}/\Delta\omega_G \approx 0.20$ [38], both starting from the reference point. The red points follow the strain contribution axis meaning that only a strain variation caused a shift of their position compared to the reference point. The orange points are shifted along the n-doping contribution axis, relatively to the red points. The relatively low slope coefficient of the n-doping contribution ($\Delta\omega_{2D}/\Delta\omega_G$) leads to a low variation of ω_{2D} with the doping compared to the variation of ω_G. Therefore, ω_{2D} is comprised within the same range for orange and red points while ω_G is mostly greater for orange points. Thus, it explains that a clear correlation between InGaN islands positions and frequency of graphene peaks can only be made for G peak when looking at the mapping. This indicates a localised n-doping of graphene under InGaN islands. This could be possibly triggered by two different phenomena. First, a charge transfer between InGaN islands and graphene could potentially dope it locally [21,39]. Otherwise, it could be due to the introduction of a heteroatom in the graphene lattice. In our case, this would come from the introduction of nitrogen atoms inside the graphitic 2D lattice as it is known to be a n-dopant of graphene [21,34]. These atoms would also act as nucleation centres for the growth of InGaN. However, it has been reported that this n-doping process due to exposure to active nitrogen at high temperature leads to the formation of structural defects giving rise to a D peak and a broadening of G and 2D peaks [21,40,41]. When looking at the Raman spectra of graphene in either covered or uncovered areas in **Figure 4(b)**, no D peak or broadening of G and 2D peaks are observed compared to the spectrum obtained before the growth (**Figure 1(d)**). The growth process does not reveal any signs of degradation of graphene or nitrogen incorporation. Thus, it is believed that nucleation occurs via van der Waals interactions, only, between InGaN and graphene.

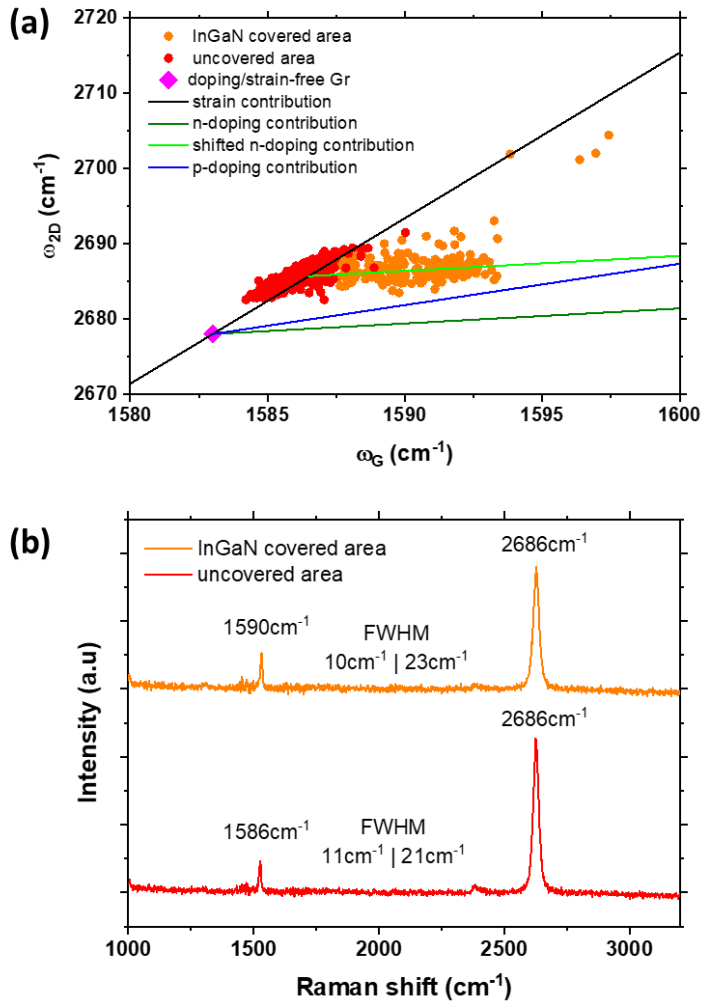

Figure 4: *(a) Distribution of 2D (ω_{2D}) and G (ω_G) peaks position for each spectrum of the Raman mapping. The doping/strain-free graphene position is indicated by a pink rotated square. The strain, p-doping and n-doping contribution axes are respectively plotted in black, blue and dark green. The light green line represents the n-doping axis shifted upward along the strain axis. (b) Raman spectra of graphene under an island (orange) and in an uncovered area (red).*

Following this first Raman mapping, the probed area was then partially scanned by AFM in contact mode. It resulted in the lateral displacement of two InGaN islands and the rotation of another one, as seen in **Figure 5(a)**, indicating a very weak bonding energy between the III-N semiconductor and the substrate. This experiment strengthens the previous assumption of a van der Waals growth process taking place during the growth of InGaN on graphene by ammonia-based MBE. On the other hand, a new Raman mapping acquired in the previous AFM scanned area **(Figure 5(b)**) reveals that the G peak position recovers its regular value in the area where InGaN islands have been moved away. We can also see that the G peak position under the rotated island, located at around x = 4 µm and y = 5 µm (x

= 5 µm and y = 6 µm in **Figure 3(b)**), has evolved according to the new orientation of the InGaN nucleus. This reversible of the G peak position, is then only due to a contact with InGaN. Indeed, the position of the characteristic peaks of the SiC substrate beneath graphene being unchanged (not displayed here), it is assumed that this shift of the G peak position cannot be caused by an additional interaction of the light with InGaN located atop.

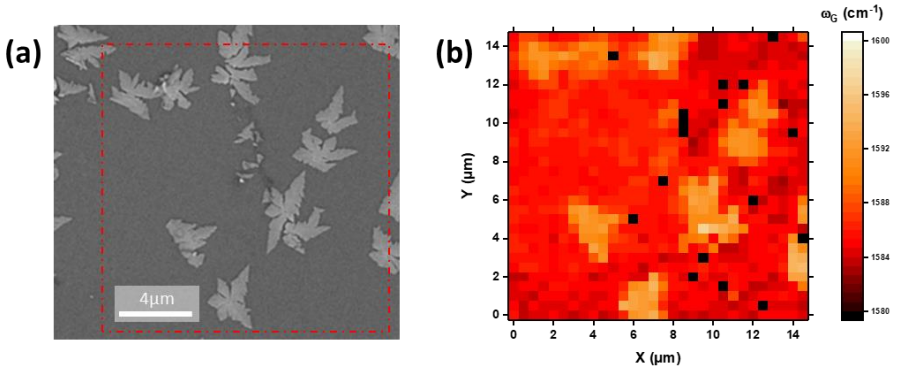

Figure 5: *(a) Secondary electron microscopy (SEM) image of InGaN nucleated at 685°C with a red dashed box indicating the area probed for the associated (b) Raman spectroscopy mapping of the G peak position (ω_G) of graphene underneath. The area considered here is the same than in Figure 3, but after the lateral displacement of few InGaN islands by atomic force microscopy (AFM) in contact mode.*

3.3 InGaN film coalescence

InGaN nucleation at 685°C has been previously demonstrated to form dendrite-like islands without damaging graphene underneath. Nucleation at 615°C showing exactly the same behaviour, this temperature was chosen to study the formation of an InGaN film with an extended growth duration while enhancing In incorporation into the alloy. In this manner, the growth of InGaN at 615°C was conducted for 2 hours resulting in an almost completely coalesced film observed by SEM in **Figure 6(a)**. The alloy seems to coalesce in some areas forming few microns long bands in the material, while it looks very disordered in the zones where there is a darker contrast in **Figure 6(a)**. It remains possible to lift off the thin film by simply using a sticky tape. When doing this and consequently scanning the area at the edge of the film and the exposed graphene, it can be observed that the coalesced bands in the material have roughly the same orientation as the terraces in the SiC substrate. However, the shape

of the InGaN bands do not exactly match the one of the terraces in the SiC. Therefore, it is not yet possible to conclude on the influence of the SiC steps on the growth of InGaN. The thickness of the film is estimated to be 70 nm, measured by AFM at the edge of an area where InGaN was removed with sticky tape. This value has to be put in perspective with the 30 nm root mean square (RMS) roughness also measured by AFM on the layer. Indeed, the measured thickness, by AFM, reaches almost 100 nm in certain regions whereas it goes down to 40 nm in others. The roughness and disorder in the film can be further evidenced by in-situ RHEED pattern along one direction of the sample as displayed in **Figure 6(b)**. The presence of dots indicates a rough layer with a 3D growth mode as observed during the nucleation and coinciding with the quite high value of RMS roughness measured. These spots are divided in three groups labelled by dark blue, green and light blue arrows in **Figure 6(b)**. The 0^{th} diffraction order is indicated by a red streak. It has to be noted that only one group of points (indicated by dark blue arrows) was visible at the early stages of the growth during the nucleation step of InGaN. Each group of spots corresponds to one family of crystallographic planes. The distance between a family of spots and the 0^{th} diffraction order being directly related to the inter-reticular distance d(h,k,l) of the planes involved in the diffraction, each family of planes can be determined. In this way, the dark blue, green and light blue arrows correspond to diffraction spots from respectively $\{10\bar{1}0\}$, $\{11\bar{2}0\}$ and $\{21\bar{3}0\}$ family of planes.

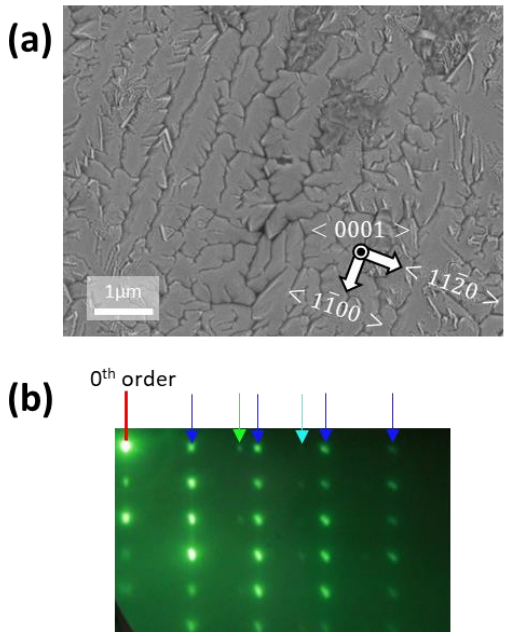

Figure 6: *(a) Secondary electron microscopy (SEM) image of the InGaN film surface after a 2 hours growth at 615°C on graphene, with white arrows indicating the crystallographic orientation of the SiC substrate. (b) Reflective high-energy electron diffraction (RHEED) pattern at the end of the growth. The red streak indicates the* 0^{th} *order of diffraction, the dark blue, green and light blue arrows respectively indicate the diffraction spots of the* $\{10\bar{1}0\}$, $\{11\bar{2}0\}$ *and* $\{21\bar{3}0\}$ *family of planes.*

In order to further investigate the several crystallographic orientations in the film, electron backscatter diffraction (EBSD) mapping was performed, with a 1° tolerance in the misorientation of the grains. The EBSD maps are shown in **Figure 7(a)**, **(b)** and **(c)**. The colorscale in **Figure 7(d)** links the colors of the maps with the corresponding reticular directions. The mapping of the out of plane orientations of InGaN (**Figure 7(b)**) exhibits two types of regions. The main region, in red in **Figure 7(b)**, corresponds to the single [0001] direction and is correlated to the bands morphology described above. This evidences a growth of the InGaN alloy along the c axis of the wurtzite structure, in majority. Small disordered areas (less than 2 µm on average) with multiple orientations are also clearly visible and correspond to the dark contrast observed on SEM image in **Figure 6(a)**. These areas are probably due to parasitic nucleation phenomena. When looking at the in-plane orientation mapping of the InGaN layer, the small disordered regions can again be easily identified because of the multiple orientations, but in the coalesced band regions, multiple orientations are also visible. The dark blue, green and light

blue colors correspond respectively to the $[10\bar{1}0]$, $[11\bar{2}0]$ and $[21\bar{3}0]$ directions of the crystallographic structure. These directions are perpendicular to the planes with the same indexes evidenced on the RHEED pattern in **Figure 6(b)**. **Figure 7(e)** helps visualising these directions in the hexagonal lattice as well as the rotation angles between them. The angle between $[10\bar{1}0]$ and $[11\bar{2}0]$ directions is 30°, while the angle between $[21\bar{3}0]$ and $[10\bar{1}0]$ directions is 19.1° and the one between $[21\bar{3}0]$ and $[11\bar{2}0]$ directions is 10.9°. EBSD mapping allows us to also estimate the proportion of each cristallographic orientations detected in the probed area. The result of this estimation is displayed in **Figure 7(f)**, which represents the fraction of each orientations found in the map according to its misorientation angle. Three peaks can be fitted with lorentzian functions attesting three different orientations in the film. A crystallographic orientation ($[21\bar{3}0]$ in light blue) appears to be dominant compared to the other two. A 10.4° misorientation angle is found between this orientation and the second most important one ($[11\bar{2}0]$ in green). Finally, a 20.2° misorientation angle is found between the main direction ($[21\bar{3}0]$) and the third one ($[10\bar{1}0]$ in dark blue). These values are consistent with the theoretical misorientation angles shown in **Figure 7(e)**, according to the 1° tolerance in the misorientation of the grains calculated by the analysis software.

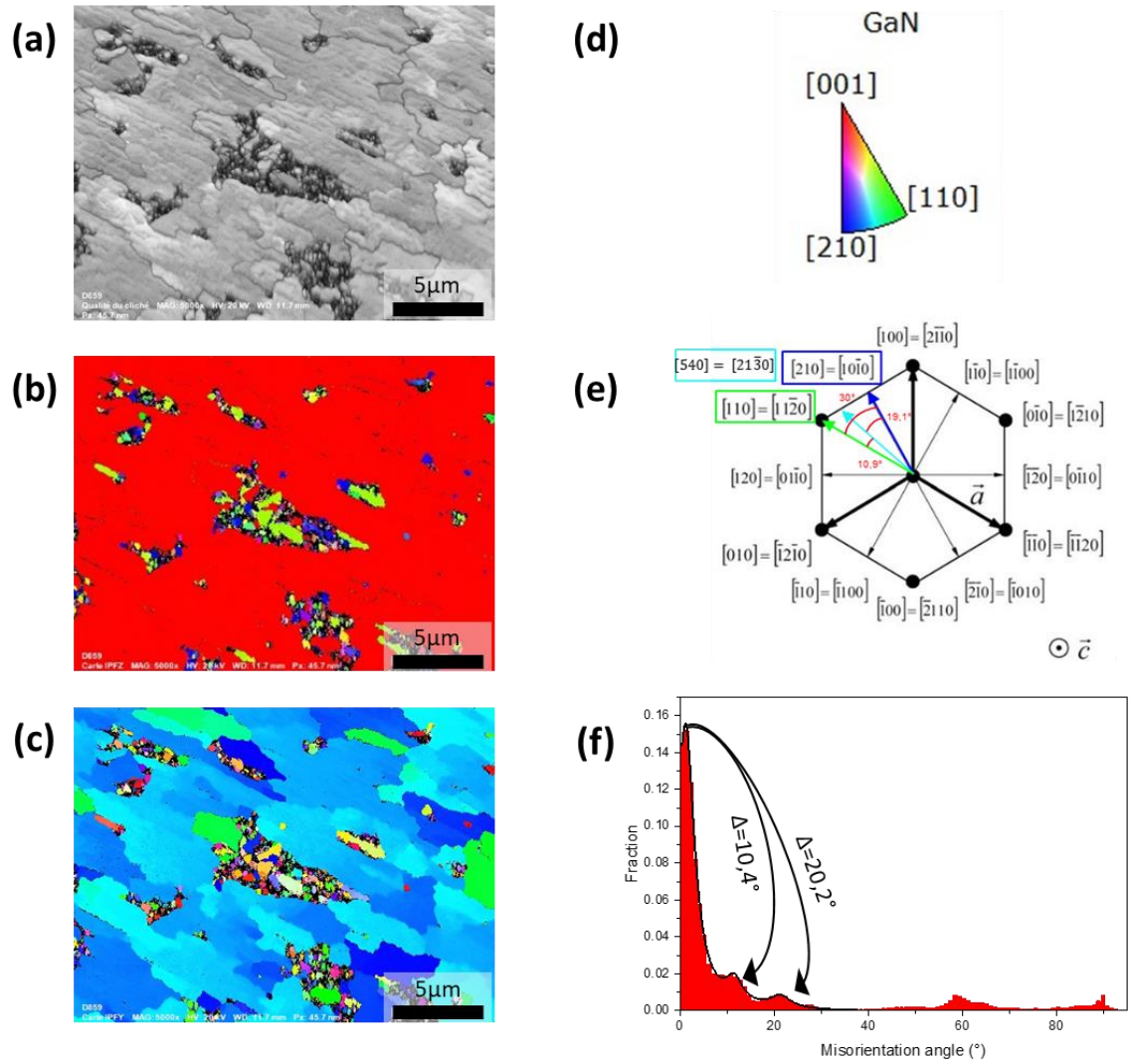

***Figure 7**: Electron backscatter diffraction (EBSD) mapping of InGaN film, grown at 615°C for 2 hours, at 20kV: (a) pattern quality, (b) out of plane and (c) in-plane crystallographic orientations, with a 1° tolerance in the misorientation of the grains. (d) Colorscale of the electron backscatter diffraction mapping. (e) Cristallographic directions in the hexagonal lattice indexed with colors matching the electron backscatter diffraction mapping colorscale. (f) Misorientation angle distribution between the grains indexed by the electron backscatter diffraction analysis software Esprit from Bruker.*

The structural characterization of the film was furthered with XRD measurements presented in **Figure 8**. φ-scan (**Figure 8(a)**) performed on $(10\bar{1}3)$ reflection of both InGaN layer and SiC substrate exhibits six peaks in both cases testifying their six-fold symmetry. More importantly, it shows that the same reflection of the two materials arise at the same position demonstrating an epitaxial relationship. No other peaks could be observed meaning that only the most dominant orientation is visible by XRD. The rocking curve performed on the (0002) reflection of the InGaN film gives a FWHM of 515 arcsec as observed in **Figure 8(b)**. This value is similar to what is obtained for GaN grown on graphene by

metalorganic chemical vapour deposition (MOCVD) by Kong et al [6], with 660 arcsec. The fact that the layer is not completely coalesced surely plays a role in this relatively low value.

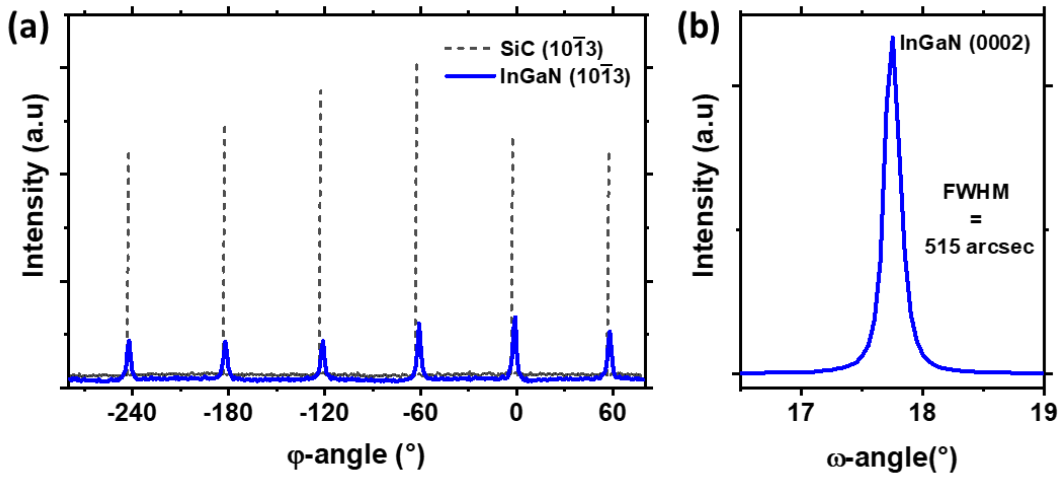

Figure 8: *X-ray diffraction measurements, (a) phi-scan performed on both InGaN layer and SiC substrate on* $(10\bar{1}3)$ *reflection and (b) rocking curve performed on InGaN on (0002) reflection.*

Finally, a PL spectrum of the sample in **Figure 9**, made at 10K, displays a band-edge emission of the alloy at 3.38 eV corresponding to 2% of In in the material according to Wu et al. [42]. The broad emission band from 2 to 3.25 eV is attributed to defects in the material.

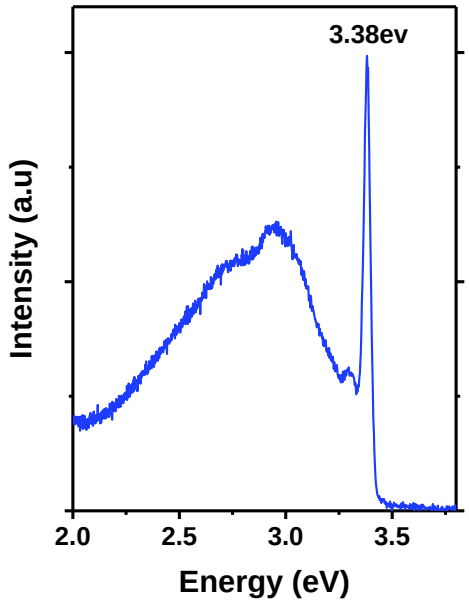

Figure 9: *Low temperature photoluminescence spectrum of the InGaN layer performed at 10K.*

4. Conclusion

To conclude, it is demonstrated the nucleation and growth of InGaN on epitaxial graphene by MBE. The growth of InGaN occurs via a 3D growth mode leading to the formation of dendritic shaped islands without damaging the graphene. A very weak binding energy between the substrate and the III-N semiconductor was evidenced by simply moving laterally InGaN nuclei on the graphene substrate by means of an AFM tip in contact mode. When extended further, the growth leads to the formation of an almost completely coalesced film. Several crystallographic orientations are found to be co-existing in the layer. The main orientation exhibits an epitaxial relationship with the SiC substrate and the quality of the film is comparable with GaN films grown on graphene already reported in literature.

Acknowledgments

The authors are grateful to J.Brault for careful reading of the manuscript and suggestions for improvements.

References

[1] Liu L and Edgar J H 2002 Substrates for gallium nitride epitaxy *Mater. Sci. Eng. R Rep.* **37** 61–127

[2] Lymperakis L, Schulz T, Freysoldt C, Anikeeva M, Chen Z, Zheng X, Shen B, Chèze C, Siekacz M, Wang X Q, Albrecht M and Neugebauer J 2018 Elastically frustrated rehybridization: Origin of chemical order and compositional limits in InGaN quantum wells *Phys. Rev. Mater.* **2**

[3] Ferrari A C et al. 2015 Science and technology roadmap for graphene, related two-dimensional crystals, and hybrid systems *Nanoscale* **7** 4598–810

[4] Plutnar J, Pumera M and Sofer Z 2018 The chemistry of CVD graphene *J. Mater. Chem. C* **6** 6082–101

[5] Manzeli S, Ovchinnikov D, Pasquier D, Yazyev O V and Kis A 2017 2D transition metal dichalcogenides *Nat. Rev. Mater.* **2** 1–15

[6] Kong W, Li H, Qiao K, Kim Y, Lee K, Nie Y, Lee D, Osadchy T, Molnar R J, Gaskill D K, Myers-Ward R L, Daniels K M, Zhang Y, Sundram S, Yu Y, Bae S, Rajan S, Shao-Horn Y, Cho K, Ougazzaden A, Grossman J C and Kim J 2018 Polarity governs atomic interaction through two-dimensional materials *Nat. Mater.* **17** 999–1004

[7] Kim Y, Cruz S S, Lee K, Alawode B O, Choi C, Song Y, Johnson J M, Heidelberger C, Kong W, Choi S, Qiao K, Almansouri I, Fitzgerald E A, Kong J, Kolpak A M, Hwang J and Kim J 2017 Remote epitaxy through graphene enables two-dimensional material-based layer transfer *Nature* **544** 340–3

[8] Kim J, Bayram C, Park H, Cheng C-W, Dimitrakopoulos C, Ott J A, Reuter K B, Bedell S W and Sadana D K 2014 Principle of direct van der Waals epitaxy of single-crystalline films on epitaxial graphene *Nat. Commun.* **5** 1–7

[9] Ayari T, Sundaram S, Li X, Alam S, Bishop C, El Huni W, Jordan M B, Halfaya Y, Gautier S, Voss P L, Salvestrini J P and Ougazzaden A 2018 Heterogeneous Integration of Thin-Film InGaN-Based Solar Cells on Foreign Substrates with Enhanced Performance *ACS Photonics* **5** 3003–8

[10] Li T, Liu C, Zhang Z, Yu B, Dong H, Jia W, Jia Z, Yu C, Gan L and Xu B 2018 GaN epitaxial layers grown on multilayer graphene by MOCVD *AIP Adv.* **8** 045105

[11] Gupta P, Rahman A A, Hatui N, Gokhale M R, Deshmukh M M and Bhattacharya A 2013 MOVPE growth of semipolar III-nitride semiconductors on CVD graphene *J. Cryst. Growth* **372** 105–8

[12] Shon J W, Ohta J, Ueno K, Kobayashi A and Fujioka H 2014 Fabrication of full-color InGaN-based light-emitting diodes on amorphous substrates by pulsed sputtering *Sci. Rep.* **4** 1–4

[13] Chen Z, Liu Z, Wei T, Yang S, Dou Z, Wang Y, Ci H, Chang H, Qi Y, Yan J, Wang J, Zhang Y, Gao P, Li J and Liu Z 2019 Improved Epitaxy of AlN Film for Deep-Ultraviolet Light-Emitting Diodes Enabled by Graphene *Adv. Mater.* **31** 1807345

[14] Kumaresan V, Largeau L, Madouri A, Glas F, Zhang H, Oehler F, Cavanna A, Babichev A, Travers L, Gogneau N, Tchernycheva M and Harmand J-C 2016 Epitaxy of GaN Nanowires on Graphene *Nano Lett.* **16** 4895–902

[15] Fernández-Garrido S, Ramsteiner M, Gao G, Galves L A, Sharma B, Corfdir P, Calabrese G, de Souza Schiaber Z, Pfüller C, Trampert A, Lopes J M J, Brandt O and Geelhaar L 2017 Molecular Beam Epitaxy of GaN Nanowires on Epitaxial Graphene *Nano Lett.* **17** 5213–21

[16] Heilmann M, Munshi A M, Sarau G, Göbelt M, Tessarek C, Fauske V T, van Helvoort A T J, Yang J, Latzel M, Hoffmann B, Conibeer G, Weman H and Christiansen S 2016 Vertically Oriented Growth of GaN Nanorods on Si Using Graphene as an Atomically Thin Buffer Layer *Nano Lett.* **16** 3524–32

[17] Zheng Y, Wang W, Li Y, Lan J, Xia Y, Yang Z, He X and Li G 2019 Self-Integrated Hybrid Ultraviolet Photodetectors Based on the Vertically Aligned InGaN Nanorod Array Assembly on Graphene *ACS Appl. Mater. Interfaces* **11** 13589–97

[18] Journot T, Okuno H, Mollard N, Michon A, Dagher R, Gergaud P, Dijon J, Kolobov A V and Hyot B 2019 Remote epitaxy using graphene enables growth of stress-free GaN *Nanotechnology* **30** 505603

[19] Al Balushi Z Y, Miyagi T, Lin Y-C, Wang K, Calderin L, Bhimanapati G, Redwing J M and Robinson J A 2015 The impact of graphene properties on GaN and AlN nucleation *Surf. Sci.* **634** 81–8

[20] Mun D-H, Bae H, Bae S, Lee H, Ha J-S and Lee S 2014 Stress relaxation of GaN microstructures on a graphene-buffered Al2O3 substrate *Phys. Status Solidi RRL – Rapid Res. Lett.* **8** 341–4

[21] Sarau G, Heilmann M, Bashouti M, Latzel M, Tessarek C and Christiansen S 2017 Efficient Nitrogen Doping of Single-Layer Graphene Accompanied by Negligible Defect Generation for Integration into Hybrid Semiconductor Heterostructures *ACS Appl. Mater. Interfaces* **9** 10003–11

[22] Nie S, Lee C D, Feenstra R M, Ke Y, Devaty R P, Choyke W J, Inoki C K, Kuan T S and Gu G 2008 Step formation on hydrogen-etched 6H-SiC{0001} surfaces *Surf. Sci.* **602** 2936–42

[23] Emtsev K V, Speck F, Seyller T, Ley L and Riley J D 2008 Interaction, growth, and ordering of epitaxial graphene on SiC{0001} surfaces: A comparative photoelectron spectroscopy study *Phys. Rev. B* **77** 155303

[24] Riedl C, Coletti C and Starke U 2010 Structural and electronic properties of epitaxial graphene on SiC(0\hspace0.167em0\hspace0.167em0\hspace0.167em1): a review of growth, characterization, transfer doping and hydrogen intercalation *J. Phys. Appl. Phys.* **43** 374009

[25] Ferrari A C and Basko D M 2013 Raman spectroscopy as a versatile tool for studying the properties of graphene *Nat. Nanotechnol.* **8** 235–46

[26] Fromm F, Jr M H O, Molina-Sánchez A, Hundhausen M, Lopes J M J, Riechert H, Wirtz L and Seyller T 2013 Contribution of the buffer layer to the Raman spectrum of epitaxial graphene on SiC(0001) *New J. Phys.* **15** 043031

[27] Landois P, Wang T, Nachawaty A, Bayle M, Decams J-M, Desrat W, Zahab A-A, Jouault B, Paillet M and Contreras S 2017 Growth of low doped monolayer graphene on SiC(0001) via sublimation at low argon pressure *Phys. Chem. Chem. Phys.* **19** 15833–41

[28] Wundrack S, Momeni Pakdehi D, Schädlich P, Speck F, Pierz K, Seyller T, Schumacher H W, Bakin A and Stosch R 2019 Probing the structural transition from buffer layer to quasifreestanding monolayer graphene by Raman spectroscopy *Phys. Rev. B* **99** 045443

[29] Tiberj A, Huntzinger J R, Camara N, Godignon P and Camassel J 2012 Raman spectrum and optical extinction of graphene buffer layers on the Si-face of 6H-SiC *ArXiv12121196 Cond-Mat*

[30] Bartelt M C and Evans J W 1994 Dendritic islands in metal-on-metal epitaxy I. Shape transitions and diffusion at island edges *Surf. Sci.* **314** L829–34

[31] Ni Z H, Yu T, Lu Y H, Wang Y Y, Feng Y P and Shen Z X 2009 Uniaxial Strain on Graphene: Raman Spectroscopy Study and Band-Gap Opening *ACS Nano* **3** 483–483

[32] Casiraghi C, Pisana S, Novoselov K S, Geim A K and Ferrari A C 2007 Raman fingerprint of charged impurities in graphene *Appl. Phys. Lett.* **91** 233108

[33] Stampfer C, Molitor F, Graf D, Ensslin K, Jungen A, Hierold C and Wirtz L 2007 Raman imaging of doping domains in graphene on SiO2 *Appl. Phys. Lett.* **91** 241907

[34] Panchakarla L S, Subrahmanyam K S, Saha S K, Govindaraj A, Krishnamurthy H R, Waghmare U V and Rao C N R 2009 Synthesis, Structure, and Properties of Boron- and Nitrogen-Doped Graphene *Adv. Mater.* **21** 4726–30

[35] Lee J E, Ahn G, Shim J, Lee Y S and Ryu S 2012 Optical separation of mechanical strain from charge doping in graphene *Nat. Commun.* **3** 1–8

[36] Das A, Pisana S, Chakraborty B, Piscanec S, Saha S K, Waghmare U V, Novoselov K S, Krishnamurthy H R, Geim A K, Ferrari A C and Sood A K 2008 Monitoring dopants by Raman scattering in an electrochemically top-gated graphene transistor *Nat. Nanotechnol.* **3** 210–5

[37] Mueller N S, Heeg S, Alvarez M P, Kusch P, Wasserroth S, Clark N, Schedin F, Parthenios J, Papagelis K, Galiotis C, Kalbáč M, Vijayaraghavan A, Huebner U, Gorbachev R, Frank O and Reich S 2017 Evaluating arbitrary strain configurations and doping in graphene with Raman spectroscopy *2D Mater.* **5** 015016

[38] Froehlicher G and Berciaud S 2015 Raman spectroscopy of electrochemically gated graphene transistors: Geometrical capacitance, electron-phonon, electron-electron, and electron-defect scattering *Phys. Rev. B* **91** 205413

[39] Fisichella G, Greco G, Roccaforte F and Giannazzo F 2014 Current transport in graphene/AlGaN/GaN vertical heterostructures probed at nanoscale *Nanoscale* **6** 8671–80

[40] Wei D, Liu Y, Wang Y, Zhang H, Huang L and Yu G 2009 Synthesis of N-Doped Graphene by Chemical Vapor Deposition and Its Electrical Properties *Nano Lett.* **9** 1752–8

[41] Lin Y-C, Lin C-Y and Chiu P-W 2010 Controllable graphene N-doping with ammonia plasma *Appl. Phys. Lett.* **96** 133110

[42] Wu J, Walukiewicz W, Yu K M, Ager J W, Li S X, Haller E E, Lu H and Schaff W J 2003 Universal bandgap bowing in group-III nitride alloys *Solid State Commun.* **127** 411–4